 CMES, vol.10, no.2, pp.171-183, 2005

A Numerical Investigation of Boumerdes-Zemmouri (Algeria) Earthquake and Tsunami

Xiaoming Wang [1] **and Philip L.-F. Liu** [1]

Abstract: On May 21, 2003 Boumerdes-Zemmouri (Algeria) earthquake generated a small tsunami, which was recorded at several locations around the coast of Balearic Islands, Spain. Recent field studies (Meghraoui, *et al.,* 2004) and teleseismic wave analysis (Yiga, 2003) indicated that the earthquake magnitude is stronger than that suggested by the Harvard CMT solution. Moreover, the seafloor displacement is also not uniform along the rupture line. In this paper, we perform a numerical investigation to evaluate the accuracy of various suggested fault plane mechanisms. The numerical model is based on the shallow-water equations and numerical results are compared with the measured wave heights at San Antonio and Ibiza, Spain. The sensitivity of fault plane parameters is also examined. Our simulations show that the fault plane mechanism proposed by Meghraoui, *et al.* gives much better tsunami wave height predictions than that of Harvard CMT solution, although some discrepancies still exist. Using an inversion method with the tide gage measurements at San Antonio, we further improve the fault plane model, which is further validated with the data taken at Ibiza. Our new fault plane model suggests a stronger earthquake with larger seafloor uplifts.

1 Introduction

On 21 May 2003, a destructive earthquake occurred in Northern Algeria, where the Eurasian plate is subducting the African plate. The African plate is moving northwestward against the Eurasian plate with a velocity of about 6 mm per year, creating a compressional tectonic environment, in which the main shock struck the region at 18:44:30 (UTC) with its epicenter calculated at (36.93^{o}N, 3.58^{o}E), 15km offshore of Zemmouri. The initial estimate of the magnitude of the earthquake is M_w= 6.8 with a seismic moment of 2.01×10^{19}Nm (2.01×10^{26}dyne-cm) and the fault plane was described with strike angle = 57^o, dip angle = 44^{o}and slip angle = 71^o (Harvard CMT solution). The province of Boumerdes, including the coastal city of Boumerdes and the Eastern district of the capital city of Algiers, were impacted by the earthquake.

Widespread damage was reported in an area about 100km long and 35km wide centered on the city of Boumerdes. The earthquake caused at least 2,266 people killed, 10,261 injured, 150,000 homeless and more than 1,243 buildings damaged. The total affected population was about 3.5 million and the overall economic lost was estimated as high as 1.5 billion US dollars (USGS, 2003).

A small tsunami was generated by this earthquake, which swept through the entire Mediterranean Sea. The tsunami struck Balearic Islands 40 to 60 minutes after the main shock. 1 to 3-meter harbor oscillations were reported, which damaged hundreds of boats in harbors. Tsunami waves were also recorded on several tide gages throughout the Mediterranean Sea, e.g., at Ibiza and San Antonio, Spain.

Recent field studies (Meghraoui, *et al.,* 2004) and teleseismic wave analysis (Yiga, 2003) have suggested that the earthquake magnitude should be stronger than that indicated by the Harvard CMT solution. In this paper, we perform a series of numerical simulations for tsunami generation and propagation based on different suggested fault plane mechanisms. Numerical results for tsunami wave heights are compared with the available tide gage measurements around Balearic Islands. Our numerical results reveal huge discrepancies between numerical results and the measurements. A series of sensitivity tests are also made to evaluate the effects of the uncertainties of fault plane parameters on the tsunami wave height predictions (in Appendix). It turns out that if the fault plane parameters are within their reasonable uncertainty range, the large differences between the calculated and measured wave heights can not be accounted for by using the uncertainty argument. We hypothesize that the fault plane mechanism could be further refined by directly using the tide gage data. An inversion method is introduced

[1] School of Civil and Environmental Engineering, Cornell University, Ithaca, New York 14853

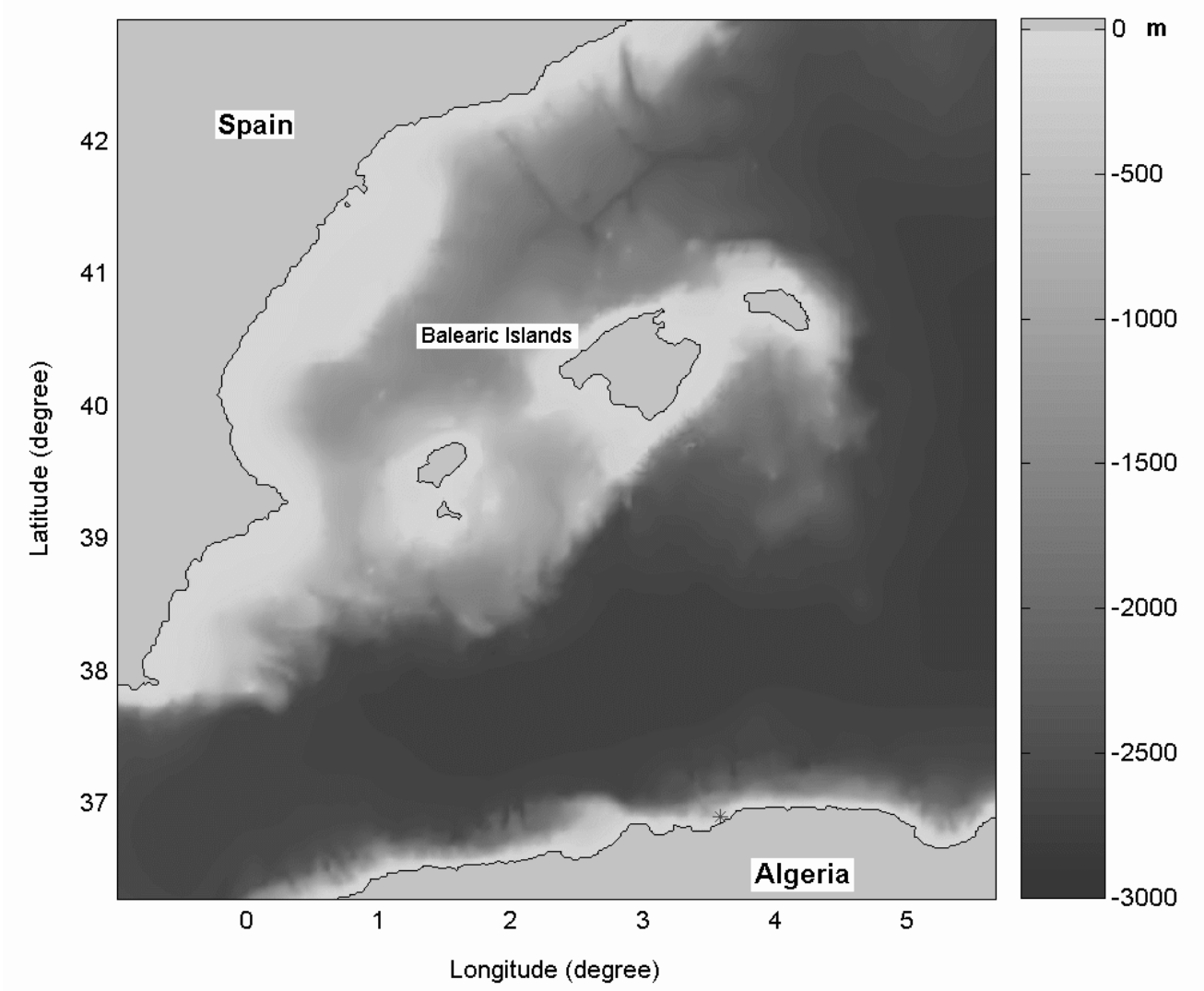

Figure 1 : Balearic Islands and bathymetry in the Mediterranean Sea. The red star shows the epicenter of May 21, 2003 Algeria earthquake

to determine the optimal estimate of the fault plane mechanism based on the tide gage data at San Antonio, Spain. The numerical results obtained by using the optimized fault plane model are further validated with the tide gage data at Ibiza, Spain.

2 Fault Plane Models

One of the most important factors, determining whether tsunami propagation can be successfully simulated and the tsunami arrival times at different locations can be accurately predicted, is the correct description of the fault plane mechanism. In general, the relationship between the tsunami generation and the fault plane mechanism can be classified into two models: Transient fault plane model and impulsive fault plane model. An impulsive fault plane model assumes that the seafloor deforms instantaneously and the entire fault line also ruptures simultaneously. Assuming that the water is incompressible, the sea surface deforms instantaneously and mimics the seafloor displacement. On the other hand, in the transient fault plane models, the seafloor deformation and the rupture along the fault line are both described as transient processes. The time history of the water depth changes will enter directly into the tsunami simulation model.

For the 2003 Boumerdes-Zemmouri earthquake, the analysis of teleseismic waves shows that the rupture mo-

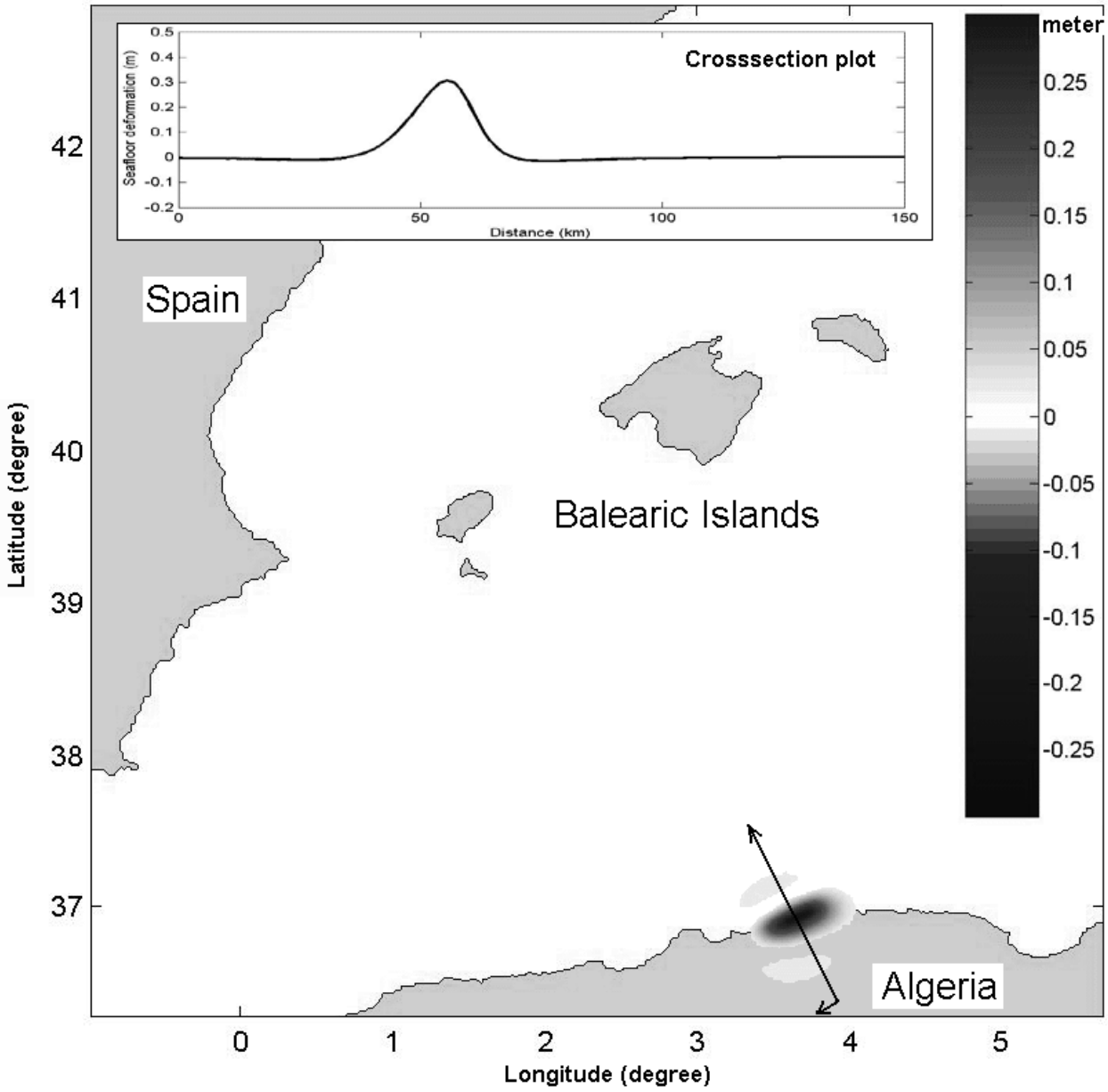

Figure 2 : The location and profile of the seafloor deformation (from Harvard CMT solution)

tions only lasted for 12 seconds (Delouis, 2004). Therefore, the speed of the rupture is roughly 3 km/s (The length of the fault plane is roughly 36 km.), which is at least one order of magnitude faster than the speed of tsunami propagation that is about 0.14 km/s in the water depth of 2 km. Therefore, the impulsive fault plane model should adequately describe the fault motion of this earthquake.

In the following simulations, we first use the fault plane parameters corresponding to the Harvard CMT solution, which are listed in Table 1. The scalar seismic moment is calculated as 2.01×10^{19}Nm, with a rectangular fault plane of 36.5km long and 18.3km width with the dislocation of 1.0 meter (Borrero, 2003). Once these fault plane parameters are selected, a linear elastic dislocation theory can be adopted to calculate seafloor deformations (Mansinha and Smylie, 1971). The dislocation theory assumes that the slip is uniform on a rectangular fault plane embedded in an elastically homogeneous half-space. As

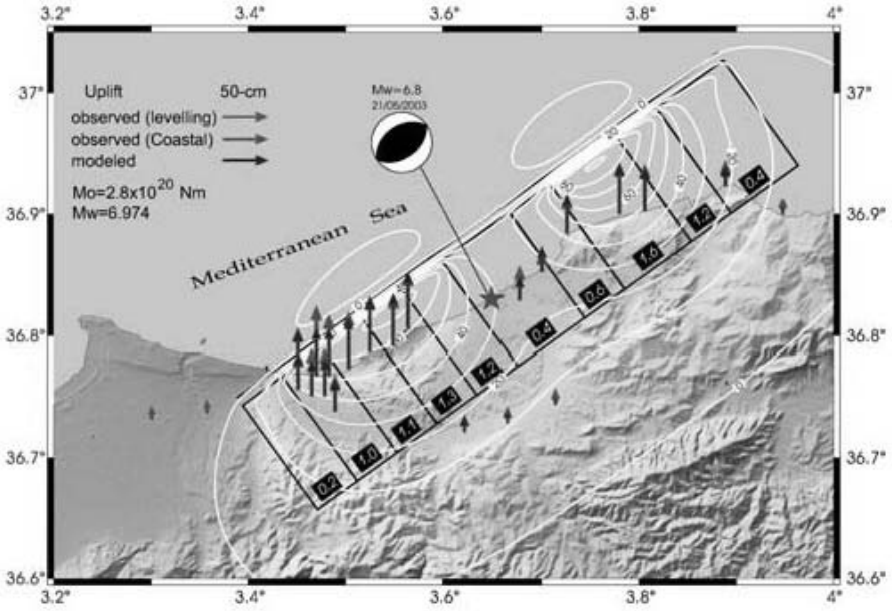

Figure 3 : Model of vertical seaflloor deformation with contours of 20 cm interval (fault model best fitting the measured uplifts, with 54^o strike angle and 50^o in dip). The amount of slip on each fault segment is shown in black boxes (Meghraoui, *et al*., 2004).

a result, the transverse profile of the calculated seafloor deformation is uniform along the fault line within the fault plane. In the following simulations, we also assume that initial sea surface deformation mimics the seafloor displacement in the source region.

On the average, the calculated seafloor uplift is about 0.30 m and there are two seafloor depression regions with the amplitude of 0.01 m, which are located on the northwestern side and the southwest side of the uplift region (See Figure 2).

However, the field survey by Meghraoui, *et al.* (2004) shows that the fault mechanism is far more complicated than the above description. They measured the uplift at 56 different locations from the difference between the uppermost white band (algae level) trace and the present-day sea level along the coastline using tape and differential GPS equipments. The measurements indicate that two major uplift regions exist along the rupture line of the earthquake, which are located to the southwest of the epicenter and to the northeast of the epicenter separately. The maximum uplift of 0.75m was found in the southwest region. Meghraoui, *et al.* (2004) also presented a fault plane model best-fitting their field measurements (see Figure 3), which is consistent with the aftershocks distribution (Bounif, *et al.,* 2004). Their best-fit model gave a seismic moment estimate of as 2.75×10^{19}Nm (equivalent to M_w 6.9).

Both fault plane models, Harvard CMT solution and Meghraoui, *et al.*'s field data, will be used to generate the initial free surface condition for simulating tsunami propagation in the Mediterranean Sea. The numerical results will be compared with the available tide gage data at Ibiza and San Antonio, Spain.

Table 1 : Fault plane parameters

Fault length	36.5 km
Fault width	18.3 km
Top depth of fault plane	10 km
Dislocation (slip)	1.0 m
Strike angle	57^0
Dip angle	44^0
Slip angle	71^0
Position of focal center (Lat, Lon)	(36.93^0 N, 3.58^0 E)

3 Numerical Simulations

The numerical model – COMCOT (Cornell Multi-grid Coupled Tsunami Model) – is used to simulate the tsunami generation and propagation. COMCOT adopts a modified leap-frog finite difference scheme to solve (both linear and nonlinear) shallow water equations. The model has been used to investigate several historical tsunami events, such as the 1960 Chilean tsunami (Liu, *et al*., 1994), the 1992 Flores Islands (Indonesia) tsunami (Liu, *et al.,* 1995) and more recently the 2004 Indian Ocean tsunami (Wang and Liu 2005).

In the western part of the Mediterranean Sea, the water depth is typically 1 km to 2 km and in the near shore regions of interest (Ibiza and San Antonio), the water depth reduces to about 5 to 10 m in the harbor. While the measured leading wave height in the harbors is about 0.4 m (In deep ocean, the wave height is much smaller.), the wavelength is in the order of magnitude of 20 km in the ocean and 5 km in the harbor region. Therefore, the tsunami propagation can be adequately described by the linear shallow water wave theory. The shallow-water equations in Cartesian coordinate system can be expressed as:

$$\begin{aligned} &\frac{\partial \zeta}{\partial t}+\frac{\partial P}{\partial x}+\frac{\partial Q}{\partial y}=0 \\ &\frac{\partial P}{\partial t}+gH\frac{\partial \zeta}{\partial x}+\tau_x H-fQ=0 \\ &\frac{\partial Q}{\partial t}+gH\frac{\partial \zeta}{\partial y}+\tau_y H+fP=0 \end{aligned} \tag{1}$$

where ζ is free surface elevation; (x,y) denote the longitude and latitude of the Earth; τ_x and τ_y are the bottom shear stress in x axis (pointing to the east) and y axis (pointing to the north); P and Q stand for the volume fluxes ($P=hu$ and $Q=hv$, with u and v being the depth-averaged velocities in longitude and latitude direction); H is the total water depth; and f represents Coriolis force coefficient. Because the size of the physical domain is not very large, in the following simulations we will not consider the effects of bottom shear stress and Coriolis force.

Using a nested grid system, COMCOT is capable of calculating the tsunami propagation in ocean and inundation in coastal zones simultaneously. For the nested grid system, the inner finer grid adopts a smaller grid size and time step size compared to its adjacent outer (larger) grid. In the outer grid, at the beginning of a time step, the volume flux is interpolated into its inner (finer) grid. And at the end of this time step, the calculated water surface elevations at the inner finer grids are averaged to update the free surface elevations of the larger grids, overlapping the finer grids, which are used to compute the volume fluxes at next time step in the coarse grids. With this method, we are able to capture nearshore features of tsunami propagation with higher grid and time resolution and at the same time maintain computational efficiency.

The simulation domain and nested grids are shown in Figure 4.

For grid *A*, the grid size is 1.5 km with a dimension of 400*400. The lower left corner of grid A is located at (0.979^{o}W, 36.270^{o}N). Grid B has a dimension of 390*510 with a grid size of 150 m (Data of grid A and B were provided by Dr. Castanedo). Grid C1 has a dimension of 495*555 with a grid size of 10 m. And grid C2 has a dimension of 210*300 with a grid size of 10 m (provided by Dr. Orfila). A reflective boundary (vertical wall) is assigned along the "shoreline" (where water depth is equal to or less than 1 m) for all grids and the radiation open boundary is adopted for boundaries falling into the water region. For each fault plane model, 3-hour physical duration of tsunami propagation has been simulated, which took about 3.5 hours CPU time on a desktop computer with 1.5GB RAM and Athlon XP 2600+ CPU.

The numerical results are compared with the available gage measurements at Ibiza and San Antonio, Spain (tidal gage measurements were provided by Dr. Castanedo). We note that the time resolution of measurements is 5 minutes at Ibiza gage and 2 minutes at San Antonio. The numerical results based on the first fault plane model (Harvard CMT solution) are shown in Figure 6. For both locations, the arrival time of the leading wave matches with measurements very well and the phases of the trailing waves also match well. However, the amplitude of numerical waves is almost 3 times smaller than that of the measured waves.

For the fault plane model based on uplift measurements by Meghraoui, *et al*. (2004), the numerical results show much better agreement with the gage data. This fault plane model predicts the amplitude of leading waves better than the first model (Figure 7), especially at San Antonio. However, the wave heights are still significantly smaller than the measured data.

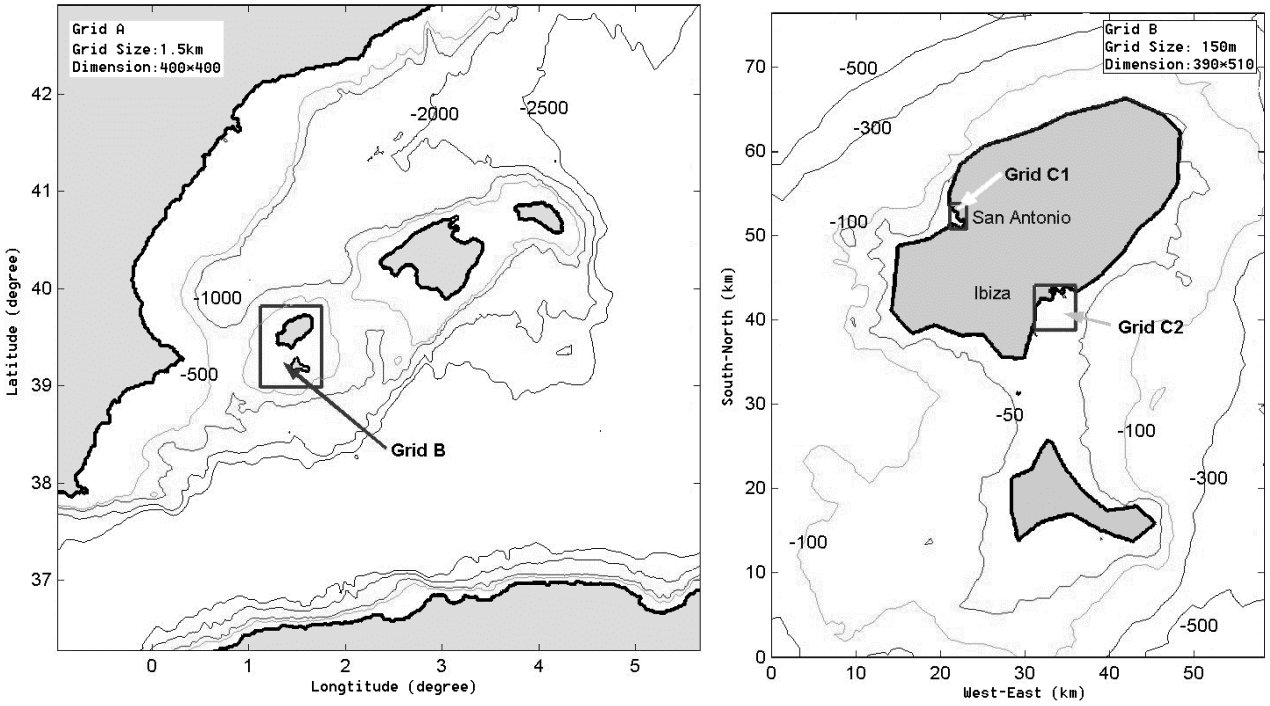

Figure 4 : Computational domains and bathymetry plots of Grid A (left panel) and Grid B (right panel).

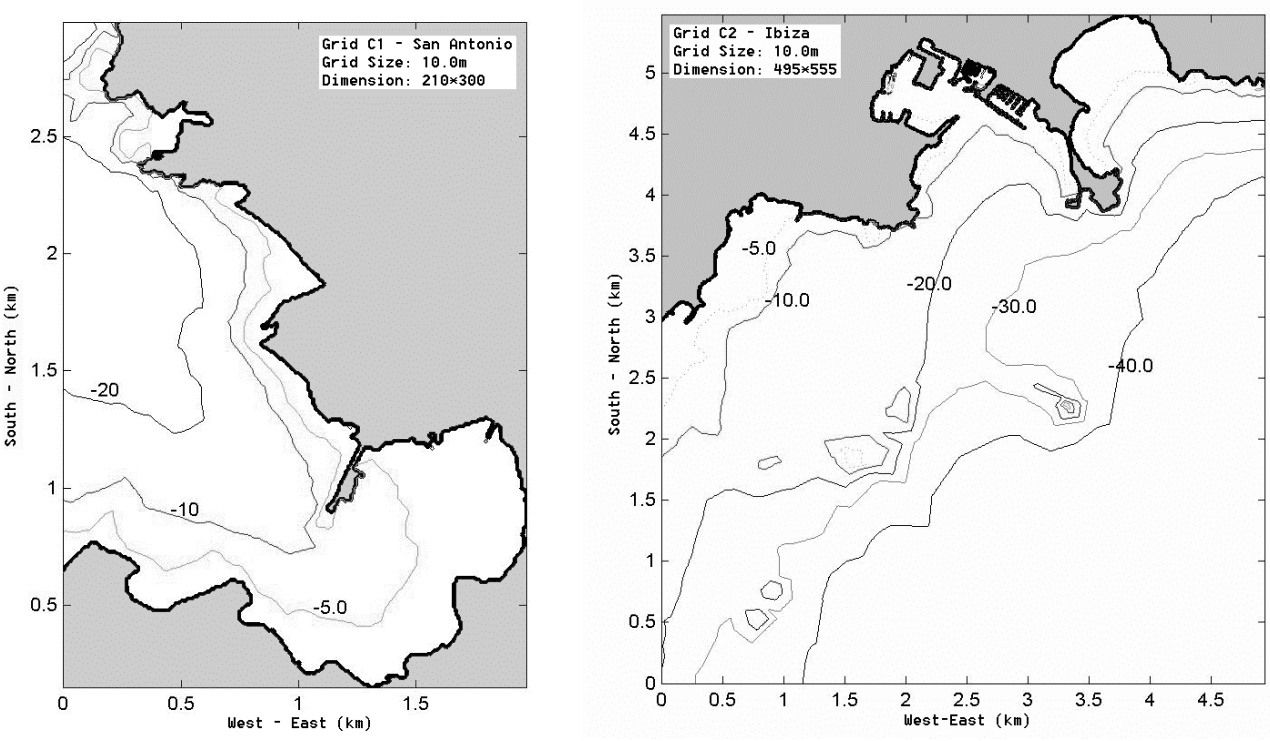

Figure 5 : Computational domains and bathymetry plots of Grid C1 (S. Antonio, left panel) and Grid C2 (Ibiza, right panel)

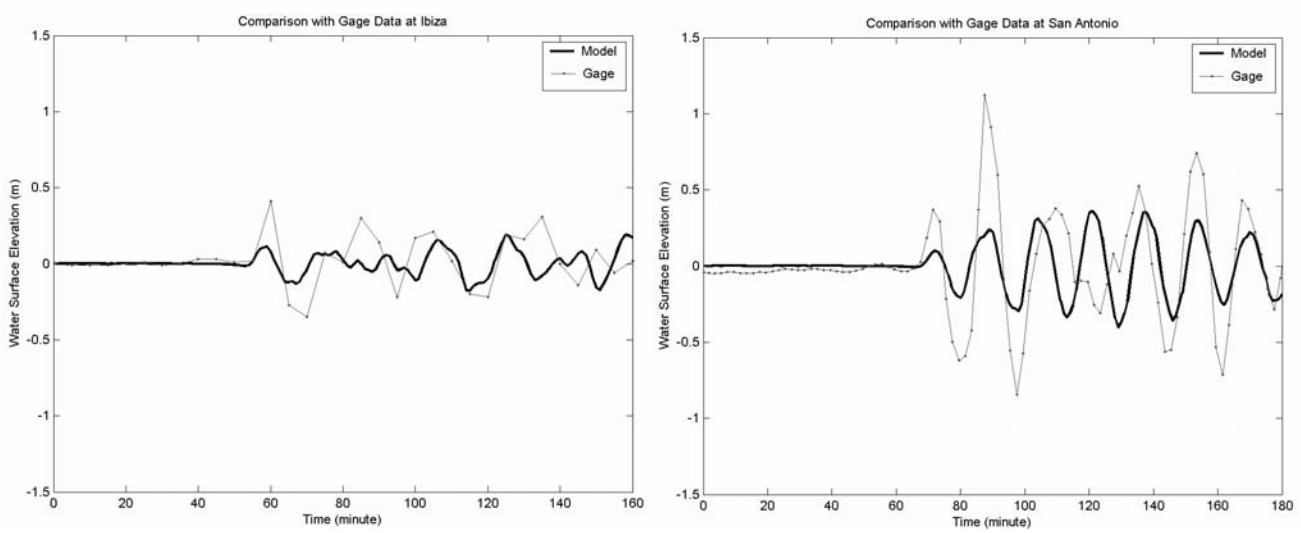

Figure 6 : Comparison between tide gage measurements and numerical results based on the fault plane model derived from the Harvard CMT solution (left: Ibiza; right: San Antonio)

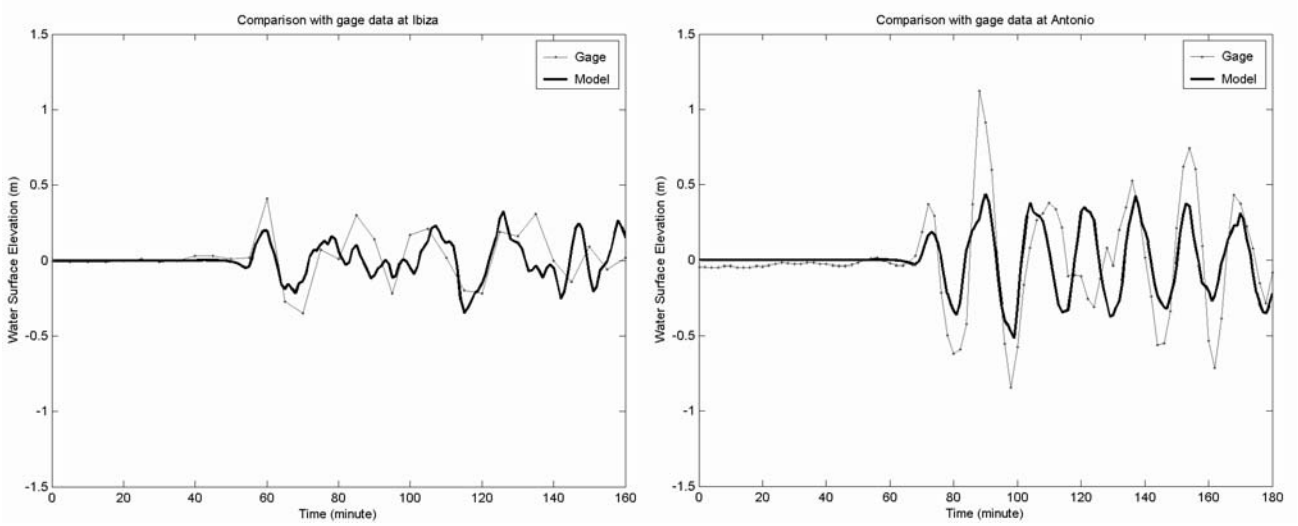

Figure 7 : Comparisons between tide gage measurements and numerical results based on Meghraoui, *et al.*'s fault plane model (left: Ibiza; right: San Antonio)

Under normal circumstances the fault plane parameters may contain a range of uncertainties, a sensitivity analysis has been performed, based on the Harvard CMT model, to evaluate if the discrepancies between the numerical predictions and the tide gage measurements of tsunami wave heights could be explained by these uncertainties. Our results show that even under the most favorable condition to the increment of the tsunami wave height, the leading tsunami wave height at Ibiza only increases by 60% (see Appendix for details). Therefore, the normal uncertainties on fault plane parameters cannot account for the differences in the calculated and measured wave heights. In the following section, an inverse method, using the tide gage data, is developed to determine the optimal seafloor displacement.

4 Optimization of Fault Plane Parameters

To improve the fault plane model, we use an optimization approach. We first outline a 60 km by 18 km fault plane according to the field observation and seismic wave analysis (Yiga, 2003; Meghraoui, *et al.,* 2004) and divide it into 6 fault plane segments. Thus each fault segment is 10 km long and 18 km width (see Figure 8).

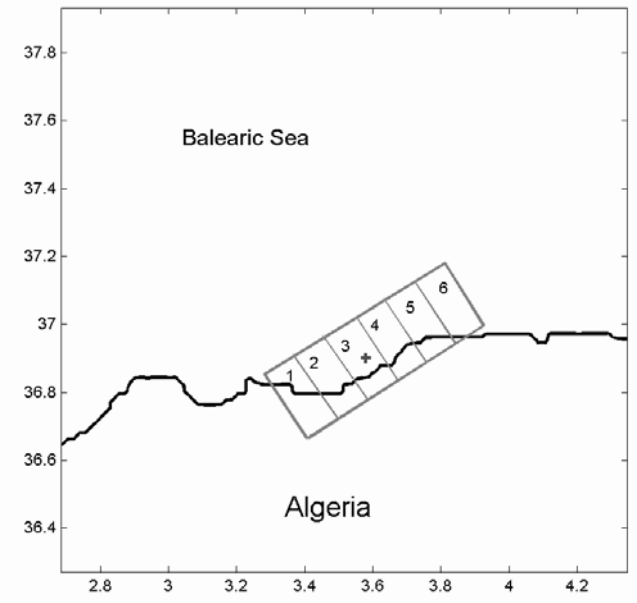

Figure 8 : Sketch of fault plane segments

Within each fault plane segment, as a starting point, the seafloor deformation is assumed to take the cross-section profile as shown in Figure 2 (i.e., the Harvard CMT solution). And it is assumed that the initial sea level distribution just mimics the seafloor deformation. Therefore, the tsunami wave field, generated by each fault segment, can be represented by a function

$$g_i = g_i(x,y,t) \tag{2}$$

where the index i (= 1, 2, 3, …., 6) denotes a fault segment, ordering from southwest to northeast. Since the tsunami simulation model is linear, the resulting temporal and spatial distribution of water surface elevations is the sum of all g_i. However, in order to minimize the error between the simulated tsunami wave heights and the tide gage data, we allow the magnitude of the seafloor deformation in the$i$ - thfault segment to be modified by a factor c_i. Thus, assuming linear relationship holds, the wave field can be expressed as

$$w(x,y,t) = \sum_{i=1}^{6} c_i g_i(x,y,t) \tag{3}$$

For a fixed location (x,y), the above function gives the time series of the free surface displacement at the position. Therefore, if the tide gage measurement at time t_j is z_j and the numerically calculated value is w_j, the optimal value of c_i can be found by minimizing $\sum_{j=1}^{N} |z_j - w_j|^2$ with nonnegative constraints, where N is the total measurements being used in the minimization. For this optimization purpose, the tide gage measurements at San Antonio are chosen since the resolution of San Antonio gage is higher than that at Ibiza. Only the measurements for the first three waves were adopted for the optimization with a total number of measurements of N = 41. In Table 2, the modification factors c_i for the seafloor deformation are listed.

Table 2 : Optimized values of amplification factor c_i

i	1	2	3	4	5	6
c_i	5.49	7.62	0.12	0	0.73	0

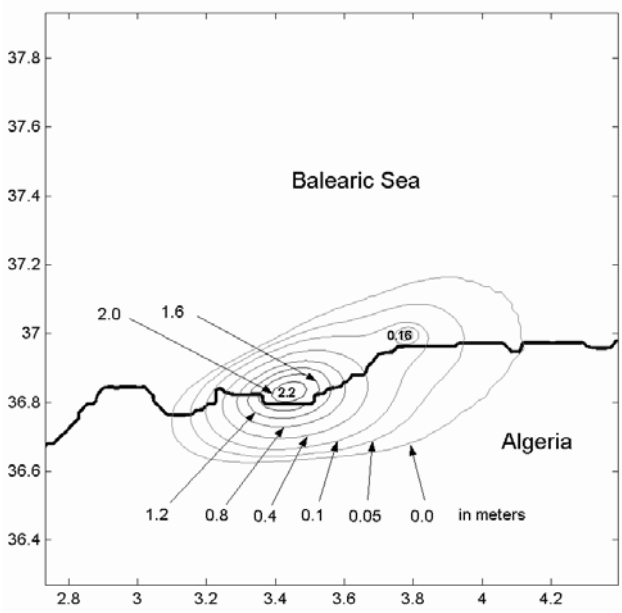

Figure 9 : Optimized seafloor deformation (Interpolation was used to smooth the deformation discontinuity between adjacent fault segments)

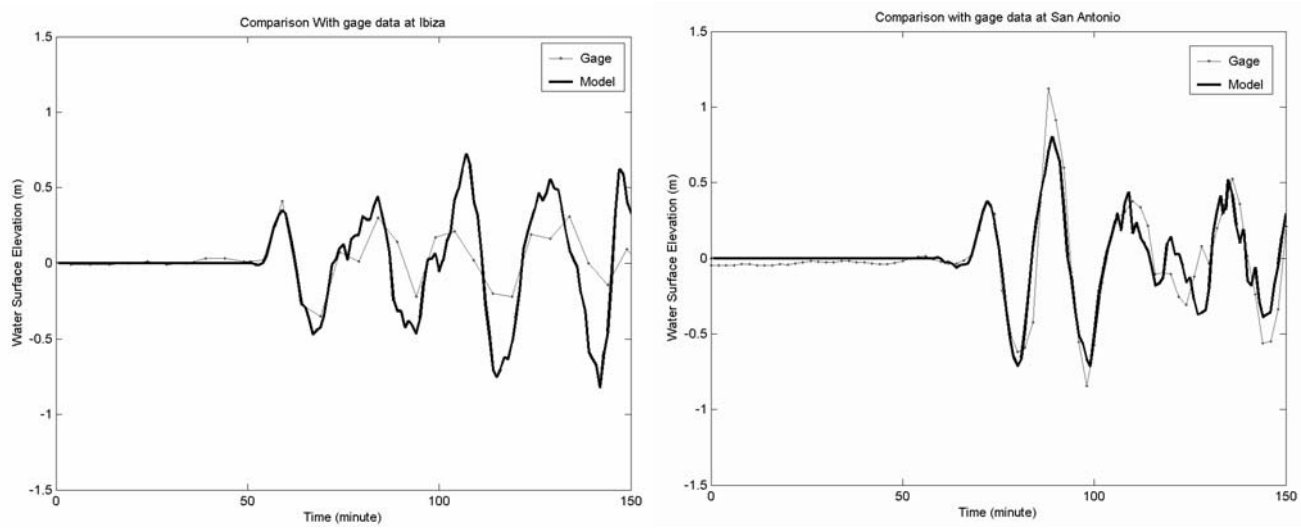

Figure 10 : Comparisons between tide gage measurements and optimized results (left: Ibiza; right: San Antonio)

Thus, the optimized seafloor deformation could be obtained by multiplying the deformation of each fault segment with a factor c_i. The contour plot of the optimized seafloor deformation is shown in Figure 9. Interpolation was used to smooth the discontinuity of seafloor deformations between adjacent fault segments.

From the optimized results, we can see that the optimized model of seafloor deformation exhibits a similar uplift pattern as the observations by Yiga (2003) and Meghraoui, *et al*. (2004). Two uplift regions can be identified from the results. Furthermore, the optimized fault mechanism gives a total scalar seismic moment of 7.92×10^{19} Nm with the rigidity μ= 3.0×10^{10} N/m^2 (corresponding to M_w= 7.2), which is much larger than the field measurements (2.75×10^{19}Nm) and the seismic wave analysis (2.4×10^{19}Nm). And most of seismic energy was released in the southwest region, covering about 95 percent of the total seismic energy.

The optimized fault plane model is further validated by the gage measurements at Ibiza (Left panel in Figure 10). The agreement for the leading wave is almost perfect.

Several snap shots of the simulated tsunami patterns, based on the optimized fault plane model, are shown in Figure 11. During the earlier stages, t = 20 min and 30 min, the tsunami spreads into the Mediterranean Sea with a small negative leading wave. Some of the tsunami wave energy is trapped along the Algerian coast; edge wave patterns are evident. Between t = 40 min and 50 min the leading tsunami wave has reached the Balearic Islands and complex diffraction and refraction patters are formed. It is noticed that the wave length decreases significantly as the tsunami waves climb up to the continental shelf.

5 Concluding remarks

In this paper, we have performed a series of numerical simulations for the 2003 Boumerdes-Zemmouri (Algeria) earthquake-generated tsunami in the Mediterranean Sea, based on the fault plane models from the Harvard CMT solution and the field measurements by Meghraoui, *et al.* (2004). The numerical results show that both fault plane models predict the tsunami arrival times at Ibiza and San Antonio, Spain very well, but greatly underestimate the leading tsunami wave heights in comparison with the tide gage data at the same locations. Through a sensitivity analysis, we conclude that the discrepancies between the tide gage data and the simulated numerical results can not be explained by the normal range of uncertainties in fault plane parameters. We then propose to find a better estimate of the fault plane parameter by using directly the tide gage measurements. An inverse method is introduced, which uses the tide gage data at San Antonio. The optimized fault plane model shows that a larger seismic moment (M_w= 7.2) is necessary to generate the tsunami wave heights observed at Ibiza and San Antonio. Moreover, the optimized fault plane model shows that about 95 percent of seismic moment was released in the uplift region southwest of the epicenter.

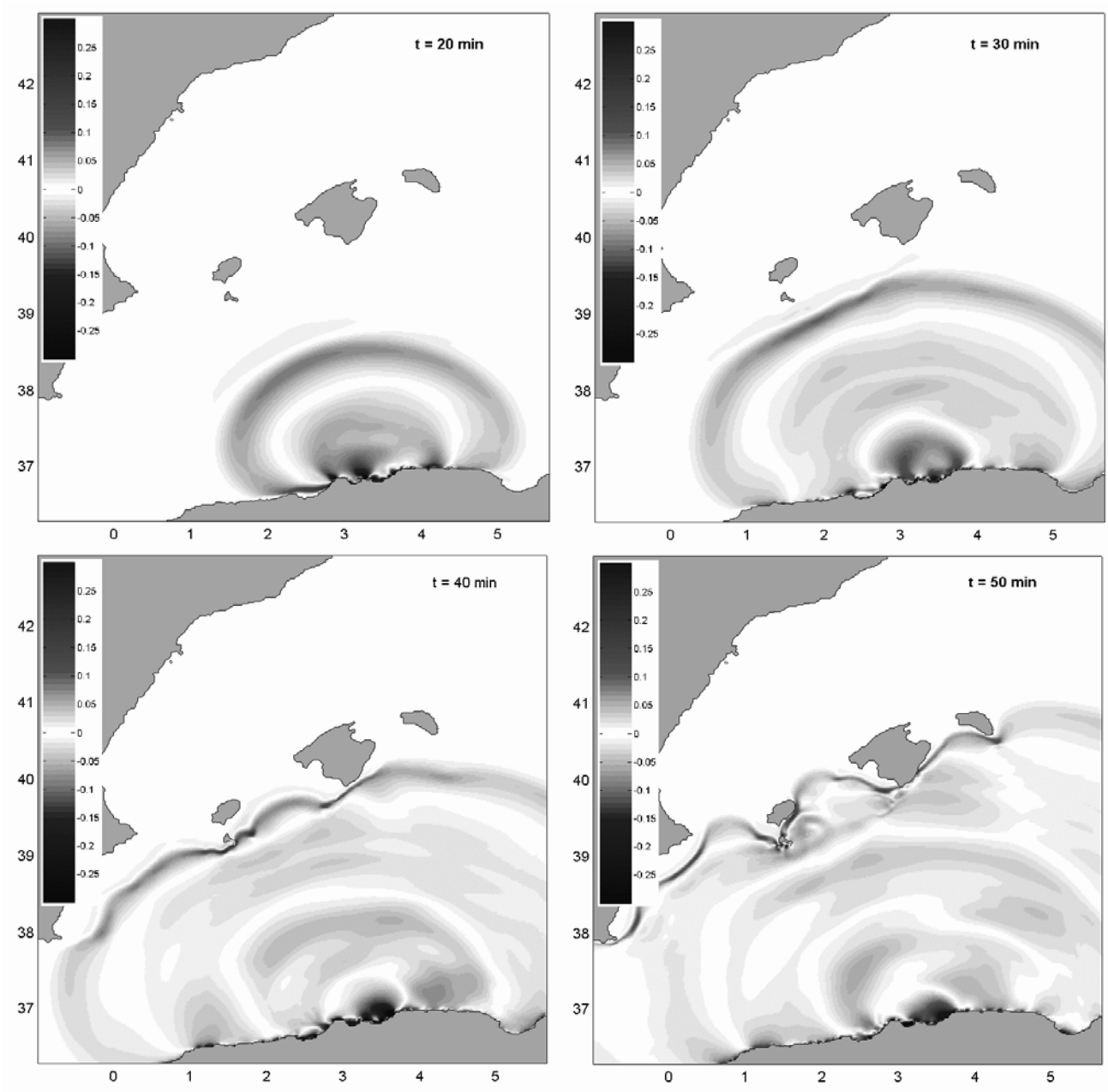

Figure 11 : Snapshots of numerically simulated tsunami waves at 20 minutes (upper left panel), 30 min (upper right panel), 40 minutes (lower left panel) and 50 minutes (lower right panel) after the earthquake struck. The colors indicate the numerically simulated free surface elevation in meter.

Acknowledgement: This paper is dedicated to Dr. Cliff Astill, who was a former program director of the Geo-hazard mitigation program at National Science Foundation. In the past fifteen years, Dr. Astill supported and encouraged many of us in pursuing tsunami research. Because of his efforts several tsunami simulation models, including the COMCOT reported herein, have been developed and are being used in the tsunami warning system and in producing tsunami inundation maps in the US. We would also like to thank our Spanish colleagues, Dr. S. Castanedo and Dr. A. Orfila for their efforts in providing field data. Research supports from NOAA, University of Alaska, and National Foundation are also acknowledged.

References

Castanedo, S. (2003): Personal communication. Also see: http://www.gioc.unican.es/presentacion/Personal/per_sonia.htm

Borrero, J.C. (2003): *Preliminary Simulations of the Algerian Tsunami of 21 May, 2003 in the Balearic Islands*. http://www.usc.edu/dept/tsunamis/ALGERIA/.

Bounif, A.; Dorbath, C.; Ayadi, A.; Meghraoui, M.; Beldjoudi, H.; Laouami, N.; Frogneux, M.; Slimani, A.; Alasset, P.J.; Kharroubi, A.; Ousadou, F.; Chikh, M.; Harbi, A.; Larbes, S. and Maouche, S. (2004): "The 21 May 2003 Zemmouri (Algeria) earthquake Mw 6.8: Relocation and aftershock sequence analysis". *Geophys. Res. Lett.*, **31**, L19606, doi:10.1029/2004GL020687.

Delouis, B.; Vallée, M.; Meghraoui, M.; Calais, E.; Maouche, S.; Lammali, K.; Mahsas, A.; Briole, P.; Benhamouda, F. and Yelles, K. (2004): Slip distribution of the 2003 Boumerdes-Zemmouri earthquake, Algeria, from teleseismic, GPS, and coastal uplift data, *Geophys. Res. Lett.*, vol. 31, L18607, doi:10.1029/2004GL020687.

Gica, E.; Teng, M.H.; Liu, P. L.-F. and Titov, V. (2005): Sensitivity Analysis of Source Parameters for Earthquake-generated Distant Tsunamis, *J. Waterway, Port, Coastal and Ocean Engrg., ASCE* (submitted).

Hartzell, S.H. and Heaton, T. H. (1983): Inversion of strong ground motion and teleseismic waveform data from the fault rupture history of the 1979 Imperial Valley, California, earthquake, *Bull. Seismol. Soc. Am*. vol. 73, pp. 1553-1583.

Jackson, J.A. (2002): Using Earthquakes for Continental Tectonic Geology, *International handbook of earthquake & engineering seismology*, Part A, pp. 491-503.

Liu, P. L.-F.; Cho, Y.-S.; Yoon, S.-B. and Seo, S.-N. (1994): Numerical simulations of the 1960 Chilean tsunami propagation and inundation at Hilo, Hawaii, *Recent Development in Tsunami Research*, Edited by M. I. El-Sabh, Kluwer Academic Publishers. pp. 99-115.

Liu, P. L.-F.; Cho, Y.-S.; Briggs, M. J.; Synolakis, C.E. and Kanoglu, U. (1995): Run-up of Solitary Waves on a Circular Island, *J. Fluid Mechanics*, vol. 302, pp. 259-285.

Mansinha, L. and Smylie, D. E. (1971): The displacement fields of inclined faults, *Bull. Seism. Soc. Am*. vol. 61, pp. 1433-1440.

Meghraoui, M.; Maouche, S.; Chemaa, B.; Cakir, Z.; Aoudia, A.; Harbi, A.; Alasset, P.J.; Ayadi, A.; Bouhadad, Y. and Benhamouda, F. (2004): Coastal uplift and thrust faulting associated with the Mw=6.8 Zemmouri (Algeria) earthquake of 21 May, 2003, *Geophys. Res. Lett.*, vol. 31, L19605, doi:10.1029/2004GL020466.

Orfila, A. (2003): Personal communication. Also see: http://www.imedea.uib.es/personal/ficha.php?id=417&lang=ca

USGS, (2003): http://neic.usgs.gov/neis/eq_depot/2003/eq_030521/

Wang, X. and Liu, P. L.-F. (2005): The 2004 Sumatra Earthquake and Indian Ocean Tsunami, *J. Hydraulic Research*. (submitted)

Yagi, Y. (2003): Source process of large and significant earthquakes in 2003. *Bulletin of International Institute of Seismology and Earthquake Engineering*, pp. 145-153

Appendix A: Sensitivity analysis of fault plane parameters

The fault plane parameters play different roles on determining the initial free surface elevations in the source region. In general, some uncertainties are always involved in estimating these fault plane parameters; it is useful to understand the sensitivity of each parameter on the prediction of wave heights at a distant location from the source region. More specifically, in the case of 2003 Boumerdes-Zemmouri tsunami, based on the Harvard CMT solution for the fault plane model, very large discrepancies between the predicted tsunami wave heights and the tide gage measurements are observed. One would like to determine if these differences can be explained by the uncertainties in the fault plane parameters.

In this appendix, we examine the effects of each fault plane parameter on tsunami wave heights at Ibiza by varying the parameter within its uncertainty range, while keeping other parameters fixed. The fault plane parameters investigated include the length and width of the fault plane, fault-plane dislocation, strike angle, dip angle, slip angle and focal depth. The uncertainty of water depth is also examined.

The leading tsunami wave height at Ibiza predicted by the original fault plane model, based on the Harvard CMT

Table 3 : Results of sensitivity analysis

Parameter	Uncertainty		Far field variation	
Seismic Moment, M_o	-20% ∼ + 20%	D	-21% ∼ +19%	-21% ∼ +19%
		A	-5% ∼ +10%	
Focal depth	-3 km ∼ + 3 km		+20% ∼ -16%	
Dip angle	-10^o ∼ $+10^o$		+1% ∼ -2%	
Slip angle	-10^o ∼ $+10^o$		-4.3% ∼ +3.9%	
Strike angle	-10^o ∼ $+10^o$		-7% ∼ +5%	
Water depth	-10% ∼ +10%		-2% ∼ +2%	

solution (listed in Table 1), is 0.113 m (see Figure 6), which will be used as the control to evaluate the impacts of changing fault plane parameters. Generally speaking, in this paper, if by varying a certain fault plane parameter within its uncertainty range causes more than 5 percent of changes in the predicted leading tsunami wave height at Ibiza, this fault plane parameter is considered a sensitive parameter.

Effects of seismic moment

The seismic moment of an earthquake, M_0, can be written as

$$M_0 = \mu DA = \mu DLW,$$

where D is the shear dislocation, A the area of rectangular fault plane, L and W the length and the width of the fault plane, respectively ($A = LW$) and μ the rigidity of the earth.

The seismic moment is obtained from the inversion of the seismic wave data (Stephen, 1983). Different waveform inversion methods will yield different values for seismic moment. However, under the normal circumstances, the values calculated from different methods agree to within about 10-20% (Jackson, 2002). For a fixed rigidity, this will introduce an uncertainty up to ±20%, either on the shear dislocation or on the area of the rectangular fault plane.

We first examine the effects of dislocation, D, by varying the value of dislocation ±20%. The results show that the amplitude of initial free surface displacements varies linearly with the magnitude of the dislocation and so do the leading tsunami wave heights in Ibiza (see Table 3). This indicates that the far field tsunami wave height is sensitive to the variation of the fault plane dislocation.

Then, by maintaining the fault plane dislocation a constant, we vary the rupture area, A, by ±20%. We note that in the analysis the length to width ratio is also fixed (i.e., $L/W = 2.0$). The results show that the predicted leading tsunami wave heights vary from -5% to 10% due to the change of the fault plane area by ±20% (see Table 3).

From the sensitivity analysis on the dislocation and fault plane area, it is obvious that the far field tsunami wave height at Ibiza is very sensitive to the variation of the seismic moment. The change of leading wave height may be up to 21% (due to the uncertainty on the dislocation).

Effect of dip angle, slip angle and strike angle

Under favorable conditions (e.g., a good distribution of seismic stations), the uncertainties in estimating strike, slip and dip angles are within 5-15^o; generally, ±10^o in strike and slip and ±5^o in dip (Jackson, 2002). By varying dip angle ±5^o, the leading tsunami wave height at Ibiza only changes up to 2 percent. Similarly, by varying the slip angle ±10^o, the change of leading tsunami wave height at Ibiza is less than 5%. However, the analysis shows that the leading tsunami wave height at Ibiza varies between -7% and +5% due to the change of strike angle within ±10^o uncertainty.

Therefore, the far field tsunami wave height at Ibiza is not sensitive to the variation of dip angle and slip angle within their uncertainty range. But it is sensitive to the variation of strike angle.

It should be noted that the effect of strike angle might be case-related. Gica *et al*., (2005) shows that the effect of strike angle may depend on the distance between the far field location and the source region. If the distance is so large that the source region may be considered as a point source. Then the effect of strike angle uncertainty can be neglected.

Effects of focal depth

Under favorable conditions, it is possible to estimate centroid depth to within ±3 km for earthquakes larger than

Mw = 5.5 (Jackson, 2002). Correspondingly, the uncertainty for the focal depth estimate is set to within ± 3 km. The results show that tsunami wave height at Ibiza harbor changes between -16% to +20%. Therefore, focal depth is a sensitive parameter.

Effect of water depth

For the numerical simulations performed above, the 1.5km grid was interpolated from the ETOPO2. The finer grids (150m and 10 m) were obtained from navigation charts, which are considered more accurate. Therefore, for the 1.5km grids, we need to understand how the variation of water depth will influence the far field tsunami wave height. In this sensitivity analysis, we changed the water depth at each grid in 1.5km girds by a random factor within $\pm 10\%$ during each run and we ran the simulation 50 times. This will give us a statistical estimate of the effect of water depth. The results show that the variation of the far field tsunami wave height is within $\pm 2\%$. Therefore, the uncertainty of water depth is not important to tsunami simulation. This is reasonable because the horizontal length scale of this type of water depth variation is one order smaller than the tsunami wavelength.

From the above sensitivity analysis, we conclude that, for the 2003 Algerian tsunami, the far field tsunami wave height is sensitive to the variation of focal depth, strike angle and seismic moment, but not sensitive to the variation of dip angle and slip angle. The variation of water depth is also not important to the prediction of tsunami wave heights.

For the overall effects of the variations of all the fault parameters, we combined the deviations of fault parameters most favorable to the increment of the tsunami wave height (i.e., increasing the shear dislocation by 20%, reducing focal depth by 3 km, decreasing dip angle by 10^o, increasing slip angle by 10^o and increasing strike angle by 10^o). The far field tsunami wave height at Ibiza only increases by 60%. Therefore, the uncertainty of fault parameters with their reasonable ranges of estimation errors cannot explain the large discrepancy between the measured data and the numerical predictions for 2003 Algerian tsunami. This implies that other factors may play an important role, or there are extraordinary estimate errors for fault parameters, especially the seismic moment.